Orbital states of V trimers in $BaV_{10}O_{15}$ detected by resonant x-ray scattering

K. Takubo,[1] T. Kanzaki,[1] Y. Yamasaki,[2] H. Nakao,[2] Y. Murakami,[2] T. Oguchi,[3,4] and T. Katsufuji[1,5,6]

[1]*Department of Physics, Waseda University, Tokyo 169-8555, Japan*

[2]*Condensed Matter Research Center and Photon Factory, Institute of Materials Structure Science, High Energy Accelerator Research Organization, Tsukuba, Ibaraki 305-0801, Japan*

[3]*Institute of Scientific and Industrial Research, Osaka University, Osaka 567-0047, Japan*

[4]*CREST, Japan Science and Technology Agency, Saitama 332-0012, Japan*

[5]*Kagami Memorial Laboratory for Material Science and Technology, Waseda University, Tokyo 169-0051, Japan*

[6]*PRESTO, Japan Science and Technology Agency, Saitama 332-0012, Japan*

(Received 23 February 2012; revised manuscript received 5 July 2012; published 27 August 2012)

$BaV_{10}O_{15}$ shows a structural phase transition associated with the trimerization of V ions at $T_s = 123$ K. We investigated the orbital states of V trimers using the technique of resonant x-ray scattering (RXS) near the V K-edge absorption energy. The ratio of the intensity between the pre-edge structure ($1s$ to $3d$ transition) and the main-edge structure ($1s$ to $4p$ transition) strongly depends on the reciprocal Q position of the scattering. We found that the Q position dependence is consistent with the model of orbital ordering proposed by Pen *et al.*, [Phys. Rev. Lett. **78**, 1323 (1997)].

DOI: 10.1103/PhysRevB.86.085141 PACS number(s): 78.70.Ck, 71.15.Ap, 71.30.+h

I. INTRODUCTION

The cluster formation of transition metals as a phase transition has been investigated extensively in various transition-metal compounds. A simple example is a dimerization associated with a spin-Peierls transition,[1] where two states originating from two transition metals form a spin-singlet state in a dimer. The cluster formations composed of more than three ions were also known, such as tetramers in $MgTi_2O_4$, heptamers in AlV_2O_4, and octamers in $CuIr_2S_4$,[2] where the orbital degree of freedom plays important roles. The cluster formation of three V^{3+} ($3d^2$) ions, i.e., V trimerization, is observed in various vanadates in which V ions form triangle-based lattices, such as $LiVO_2$,[3] $LiVS_2$,[4] NaV_6O_{10},[5] $BaV_{10}O_{15}$,[6–9] $SrV_8Ga_4O_{19}$,[10] $AV_{13}O_{18}$ (A = Ba, Sr),[11] and $A_2V_{13}O_{22}$ (A = Ba, Sr).[12]

Theoretically, Pen *et al.* proposed a model of t_{2g} orbital ordering for the V trimerization in $LiVO_2$.[13] In their model, a bonding state of the t_{2g} orbitals is formed at each side of the V^{3+} triangle as shown in Fig. 1(a). Experimentally, however, such orbital ordering in the V trimer has not been confirmed yet in $LiVO_2$ because of the stacking fault along the c axis existing in the single crystal of $LiVO_2$, which prevents us from even doing a simple structural analysis. Among other vanadates showing trimerization, $BaV_{10}O_{15}$ is a compound whose large single crystals can be easily grown by a floating-zone method.[9] To investigate the orbital states in transition-metal oxides, resonant x-ray scattering (RXS) at the K edge of transition metals is an excellent probe, since it can detect both the local site symmetry and modulation of the electronic states in transition metal by the quantitative analysis of the reciprocal Q position dependence in the RXS signal.[14–17]

$BaV_{10}O_{15}$ contains V ions on the modified triangular lattices. This compound shows a structural phase transition at $T_s = 123$ K,[6–9] where the electrical resistivity sharply increases by 10^3 times. It was found that the structural change at T_s is characterized by the trimerization of the V ions over two layers,[9] as shown in Fig. 1(c) with the global a, b, and c axes, where V3B is on the $c = 3/8$ layer and V3 and V2B are on the $c = 5/8$ layer. One trimer and the neighboring oxygen ions are extracted in Figs. 1(b) and 1(a) shows the same trimer in the local $\vec{x}$, $\vec{y}$, $\vec{z}$ coordinate, each of which is along a V ion and a neighboring O ion.

In this paper, we measured the energy and azimuthal-angle dependences of RXS near the K absorption edge at various Q positions for $BaV_{10}O_{15}$. We found that the result of the model analysis about the Q dependence is consistent with the Pen's model and a band calculation.

II. EXPERIMENT

Single crystals of $BaV_{10}O_{15}$ were grown by the floating zone method, and the ac plane was cut from a single crystal. X-ray scattering measurements were performed at BL-4C at the Photon Factory of KEK. The energy of the incident x ray was around 5.48 keV, corresponding to the K edge of the absorption in the V ion. The energy resolution was ~3 eV. The incident x-ray beam had σ polarization in the present experimental configuration, as illustrated in Fig. 2(a). We measured the dependence of the resonant scattering signal on the azimuthal angle (Ψ), which is the rotational angle of the sample around the scattering vector. The origin of Ψ is defined as the configuration in which the polarization of the incident photon beam is parallel to the a axis. The electronic band structure of $BaV_{10}O_{15}$ for the low temperature phase ($pbca$ structure in Ref. 8) is calculated within the local-density approximation (LDA) to the density-functional theory with the full-potential linearized augmented plane-wave method, which has been used for several transition-metal oxide systems.[18–20]

III. RESULTS AND DISCUSSION

Figure 2(b) shows the θ–2θ scan at (050) with $\Psi = 0^\circ$ at 20 K (below T_s), together with that at (040) in the inset. The photon energy was 5.481 keV, corresponding to the main-edge structure of the V K absorption [structure C in Fig. 3(a)]. The signal at (050) is clearly observed, though its intensity is three

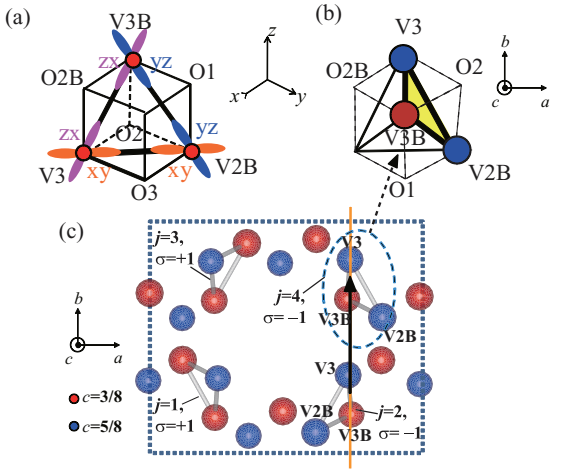

FIG. 1. (Color online) (a) Trimers in the local $\vec{x}$, $\vec{y}$, $\vec{z}$ coordinates and the model of the orbital order proposed by Pen *et al*. (Ref. 13). (b) Trimers composed of V3B, V3, and V2B sites in the crystal in the global a, b, c coordinates. (c) Arrangements of the V ions for $BaV_{10}O_{15}$. The bars connecting the circles represent the V-V bonds in trimers. The b glide on the bc plane is indicated by the solid line. The arrows denotes the glide operation of the V trimer sites.

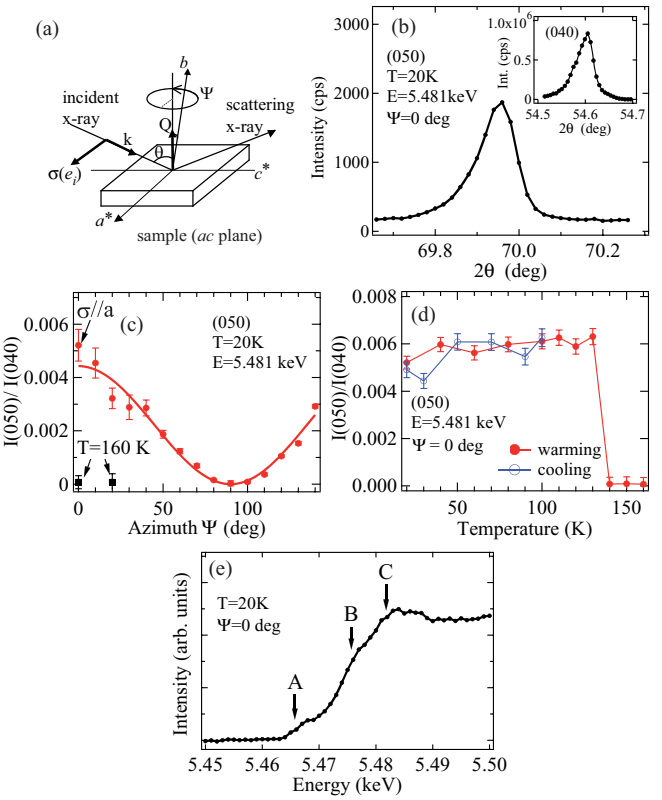

FIG. 2. (Color online) (a) Schematic view of the experimental configuration and definition of the polarization directions. (b) θ–2θ scan of the (050) resonant scattering at $\Psi = 0°$ for the main edge structure at 20 K. The inset shows the (040) diffraction taken with the same condition. (c) Azimuthal angle dependence of the RXS intensities at (050) for the main-edge structure. (d) Temperature dependence of the magnitude of RXS at (050) for the main-edge structure. (e) Fluorescence spectra near the V K edge at 20 K.

orders of magnitude smaller than that at (040). As shown in Fig. 2(c), the intensity is maximized at $\Psi = 0°$, where the polarization of the incident x ray $\vec{e}_i$ is parallel to the a axis and that of the scattered x ray $\vec{e}_s$ is approximately along the ab plane, whereas it is almost zero at $\Psi = 90°$, where $\vec{e}_i$ is parallel to the c axis and $\vec{e}_s$ is approximately along the bc plane [see Fig. 2(a)]. Here, the scattering at $(0k0)$ (k = odd number) is forbidden in the normal Thomson scattering because of the existence of the b glide on the bc plane in the crystal. However, the resonant x-ray scattering has a finite amount of intensities when the polarization of either the incident or scattered x ray is along the a axis and the polarization of the other is either along the b or c axis (see Appendix A for more details). The present azimuthal angle dependence of the (050) intensities is consistent with this, indicating that the (050) peak arises from the resonant x-ray scattering.

Figure 2(d) shows the temperature dependence of the RXS intensities. The RXS intensities are almost zero above $T_s = 123$ K, sharply increase at T_s, and barely depend on temperatures below T_s, indicating a first-order character of the phase transition.

Next, let us discuss the photon-energy dependence of RXS. As can be seen in Fig. 3(a), three distinct peak structures (labeled as A, B, and C) are observed on the photon-energy dependence of RXS at the (010), (030), and (050) reflections. For these three peaks, the relative intensities are different for different Q positions, though the energy of the peak positions are the same. We confirmed that the azimuthal angle dependence and temperature dependence were almost the same for the three structures. These three structures can be observed in the fluorescence spectra [Fig. 2(e)]. The structure A around 5.466 keV is the so-called pre-edge structure corresponding to the threshold of the $1s$ to $3d$ transition of the V sites, while the structure C around 5.481 keV is the main-edge structure corresponding to the threshold of the $1s$ to $4p$ transition.[16,17,21]

For the ion sitting at a centrosymmetric position of the octahedra, a dipole transition from $1s$ to $3d$ is prohibited but only a quadrupole transition is allowed, whose cross section is usually a few percent of the dipole cross section.[22] Thus, the intensity of the pre-edge is much weaker than that of the main edge in various vanadates. However, if the transition metal sits on a off-centrosymmetric position, there appears electric dipole, which is given by the superposition of the p states to the d state in transition metals through the hybridization with the oxygen $2p$ state. In this situation, the dipole transition between $1s$ and $3d$ hybridized with $4p$ becomes allowed.[22–24] Therefore, the large intensity of the pre-edge A in $BaV_{10}O_{15}$ is caused by the breaking of the local centrosymmetry at the V site, which is associated with the bond formation between two V ions at each edge of the V triangles.

As to the structure B around 5.476 keV, a similar but smaller structure is observed in the RXS of several vanadates, for example, V_2O_3.[17] According to the x-ray absorption spectra of VO_2 by Poumellec *et al*., the peak energy of B (∼5.476 keV) can be ascribed to the $1s$ to $4s$ transition.[25] A large intensity of the structure B in $BaV_{10}O_{15}$ should also be attributed to the off-centrosymmetric V ion in the trimer. These peak assignments are consistent with the LDA calculation shown in Fig. 4(a) . The thresholds of the $4s$ and $4p$ states are located at about

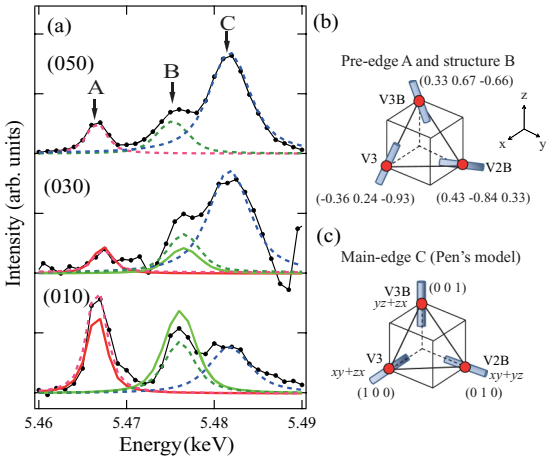

FIG. 3. (Color online) (a) Photon energy dependence of RXS at $Q = (010)$, (030), and (050). The backgrounds are subtracted using the fluorescence spectra. The fitting results for the structures A ($3d$), B ($4s$), and C ($4p$) are indicated by the dashed lines. The calculated intensities of the pre-edge A and structure B for (010) and (030) from the model analysis are also plotted (solid lines). (b) Principal axes of the ASF tensors for the $1s$ to $3d$ (pre-edge A) and to $4s$ (structure B) transition. (c) Principal axes for the $1s$ to $4p$ (main-edge C) transition in the Pen's model.

6–8 eV and 10–12 eV above the Fermi level, and these energies are comparable to the energy difference between the structure A and B or C. Furthermore, a finite amount of the $4p$ density is observed at the energy ranges of the $3d$ and $4s$ states, indicating the hybridization between these states.

As seen in Fig. 3(a), the intensity ratios of the structure A, B, and C are different for different Q positions. The energy dependences were fitted by three Lorentz-Gaussian functions (shown by dashed lines), and the intensity ratios I_A/I_C and I_B/I_C were obtained, as listed in Table I. The ratios of I_A/I_C and I_B/I_C at (010) are larger than those at (030) and (050), indicating that the pre-edge signal is enhanced at (010).

The RSX intensity is proportional to the square of the structure factor, and the contribution of the resonant process in the structure factor for $(0k0)$ at $\Psi = 0^\circ$ is given by

$$S(k) = \sum_{j,\alpha} \sigma_j f^{\alpha}_{ab} \exp(2\pi i k b_{\alpha,j}), \qquad (1)$$

where α = V3B, V3, V2B, $j = 1$ to 8 [corresponding to equivalent positions in the unit cell shown in Fig. 1(c)], σ_j is the parity multiplied for the ion at the jth equivalent position, f^{α}_{ab} is the anisotropic ab component in the atomic scattering factor (ASF) tensor of the α ion in the global a,b,c coordinates, and $b_{\alpha,j}$ is the b position of the α ion at the jth equivalent position (see Appendix A for more detailed discussions).

As can be seen in Eq. (1), the structure factor for $(0k0)$ is dominated by the ASF tensors f^{α}_{ab}, and the result that the Q dependence is different between the main-edge C and the pre-edge A (or structure B) indicates that the ASF tensor, which depends on the energy of the x ray, is different in the pre-edge A (or structure B) region and the main-edge C region. Such a difference arises from the different origins of the ASF tensors in the V ion for the pre-edge A (and structure B) and main-edge C: The ASF tensors of the pre-edge A (and

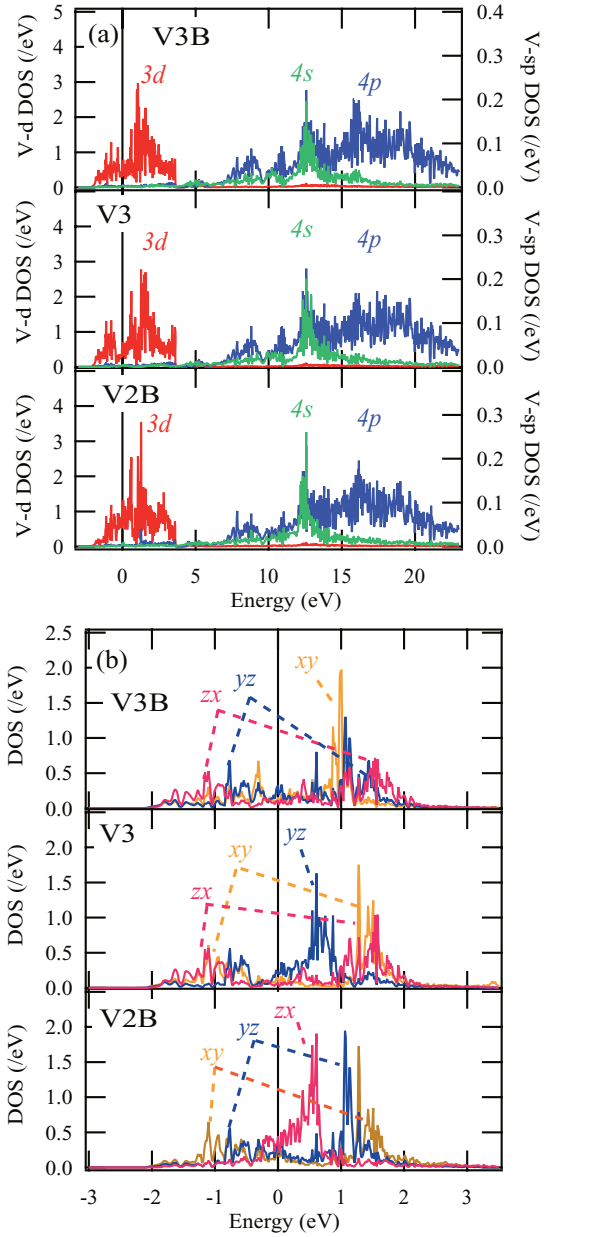

FIG. 4. (Color online) LDA densities of states (DOS) for the trimer sites of $BaV_{10}O_{15}$ in the low temperature phase. (a) Partial density of the $3d$, $4s$, and $4p$ orbitals. (b) Partial density of the xy, yz, and zx orbitals.

structure B) arise from the centrosymmetry breaking of the VO_6 octahedra, whereas those of the main-edge C arise from the splitting of the $4p$ states, which reflects the orbital ordering of the $3d$ t_{2g} state in the V ion, as discussed in the following and in more details in Appendix B.

As to the pre-edge A and structure B ($1s$ to $3d$ or $4s$), associated with the V trimerization, the electric dipole appears around the V ion, and the dipole transition from $1s$ to $3d$ or $4s$ becomes allowed. In this situation, when the electric dipole is along (p,q,r) in the global $\vec{a}$, $\vec{b}$, $\vec{c}$ coordinates, the anisotropic part of f_{ab} for the pre-edge A and structure B is proportional to the projections of this dipole to the a and b axis, $f_{ab} \propto pq$. This is equivalent to say that the principal

TABLE I. Intensity ratios of the pre-edge A and structure B to the main-edge structure C, each of which is normalized to the intensity at (050), both by experiment and calculation.

	Experiment				Calculation
Q	I_A/I_C	$\frac{I_{A(0k0)}/I_{A(050)}}{I_{C(0k0)}/I_{C(050)}}$	I_B/I_C	$\frac{I_{B(0k0)}/I_{B(050)}}{I_{C(0k0)}/I_{C(050)}}$	$\frac{I_{A(0k0)}/I_{A(050)}}{I_{C(0k0)}/I_{C(050)}}$ and $\frac{I_{B(0k0)}/I_{B(050)}}{I_{C(0k0)}/I_{C(050)}}$
(010)	1.08 ± 0.15	7.7 ± 1.7	0.77 ± 0.17	3.5 ± 1.1	6.1
(030)	0.07 ± 0.10	0.5 ± 0.8	0.17 ± 0.11	0.8 ± 0.6	0.53
(050)	0.14 ± 0.08		0.22 ± 0.09		

axis of the ASF tensor for the pre-edge A and structure B is along the electric dipole direction. The dipole direction, (p,q,r), for the V3B, V3, and V2B sites corresponds to the shift of the V atoms from the center of the octahedron, and approximately along the line connecting each corner and the center of the V triangle. Experimentally, it can be determined from the diffraction data,[7] as shown in Fig. 3(b) in the local $\vec{x}$, $\vec{y}$, $\vec{z}$ coordinates. From these values, the Q dependence of the RXS intensities for the pre-edge A and structure B can be calculated.

On the other hand, the ASF tensor for the main-edge peak C is dominated by the energy splitting of the $4p$ states, as discussed in Refs. 14,15,26, and 27. For example, when the yz and zx states of V $3d$ orbitals are occupied, the p_z state of V $4p$ orbitals is split from the p_x and p_y state, either by the Coulomb interaction[27] or the Jahn-Teller distortion of the oxygen octahedra.[26,28] In either model, the principal axis of the ASF tensor is along the local z direction. In this case, the ASF tensor in the local $\vec{x}$, $\vec{y}$, $\vec{z}$ coordinates is given as

$$\begin{pmatrix} f & 0 & 0 \\ 0 & f & 0 \\ 0 & 0 & f+\Delta f \end{pmatrix} = fI + \Delta f \begin{pmatrix} 0 & 0 & 0 \\ 0 & 0 & 0 \\ 0 & 0 & 1 \end{pmatrix}, \quad (2)$$

where I is the unit matrix. Here, we assume that f and Δf are the same for all three V sites in the trimer, though the direction of the principal axis, which is determined by the occupation of the d states as described above, is different at each V site. With this assumption, the Q dependence for the RXS intensity calculated by Eq. (1) depends only on the direction of the principal axis at each V site. In the model of the orbital ordering by Pen *et al.*, d_{zx}, d_{yz} are occupied in V3B, d_{zx}, d_{xy} are occupied in V3, and d_{yz}, d_{xy} are occupied in V2B. Therefore, the directions of the principal axes for the ASF tensors of V3B, V3, and V2B are (0,0,1), (1,0,0), and (0,1,0), respectively [see Fig. 3(b)]. From these directions, the Q dependence of RXS intensity for the main-edge C can also be calculated.

It should be noted that the Q dependence for the RXS intensity can be calculated of I_A, I_B, and I_C, but the absolute intensity for I_A, I_B, and I_C at a given Q position cannot be obtained in the present calculation, since it depends on the absolute values of f^α in Eq. (1), which are not taken into account in the present analysis. Namely, only $I_{(0k0)}/I_{(050)}$ can be obtained in the calculation. On the other hand, the absolute intensities at different Q positions are difficult to compare experimentally because of the different scattering angles,[29] and only I_A/I_C and I_B/I_C can be discussed in the experiment. Thus, we normalized the intensity at (010) and (030) to that at (050) for each of I_A, I_B, and I_C, and take the ratio of the two. Namely, $[I_{A(0k0)}/I_{A(050)}]/[I_{C(0k0)}/I_{C(050)}]$ and $[I_{B(0k0)}/I_{B(050)}]/[I_{C(0k0)}/I_{C(050)}]$ were obtained for (010) and (030) both in the experiment and calculation (Table I). The calculated I_A and I_B for (010) and (030), are also plotted by solid lines in Fig. 3(a). As can be seen, the experimentally obtained values of $[I_{A(0k0)}/I_{A(050)}]/[I_{C(0k0)}/I_{C(050)}]$ and $[I_{B(0k0)}/I_{B(050)}]/[I_{C(0k0)}/I_{C(050)}]$ at (010) and (030) are well reproduced by the present model with the orbital ordering proposed by Pen *et al.* It is to be noted that this model is also consistent with the recent ^{51}V NMR study of $BaV_{10}O_{15}$.[30]

The orbital occupancies can also be discussed in the LDA calculation from the splitting of the density of the state (DOS). For example, quite large splittings of DOS are observed for the d_{xy} and d_{yz} states in the V2B site, and the lower states of them are occupied, whereas the higher states are unoccupied [Fig. 4(b)]. On the other hand, the splitting of the d_{zx} state is barely observed and is located in the unoccupied region. This means that d_{xy} and d_{yz} states are preferably occupied in the V2B site. In a similar manner, d_{zx}, d_{yz} are preferably occupied in V3B and d_{zx}, d_{xy} are occupied in V3. These orbital arrangements are the same as the Pen's model [Fig. 1(a)] and consistent with the RXS result.

IV. SUMMARY

We have observed the RXS of $BaV_{10}O_{15}$ in the V K-edge region below $T_s = 123$ K. Three peak structures are observed on the photon-energy dependence of RXS. The intense peak structures of the pre-edge A and structure B indicate the local centrosymmetry breaking of the V octahedra. The Q position dependences of RXS are consistent with the model of orbital ordering by Pen *et al.* and an LDA calculation.

ACKNOWLEDGMENTS

We thank T. Mizokawa for fruitful discussions. This work was partly supported by Grant-in-Aids for Scientific Research on Priority Areas (20046014) from MEXT and Scientific Research B (19340102) from JSPS of Japan, and Scientific Research S (21224008), by JSPS, FIRST program, and by JST, CREST. K.T. acknowledges support of JSPS for the Young Scientists (21-7913). The synchrotron radiation experiments were performed at the BL-4C in the KEK with the approval of the Photon Factory Program Advisory Committee (Proposal No. 2009S2-008).

APPENDIX A: DETAILED FORM OF THE STRUCTURE FACTOR IN THE RXS SCATTERING

1. Structural factor and the atomic scattering factor (ASF) tensor

In general, the structure factor of the resonant x-ray scattering (RXS) is given as

$$S(k) = \sum_{j=(u.c.)} \vec{e}_s \cdot \hat{f}_j \cdot \vec{e}_i \exp(i\vec{K} \cdot \vec{d}_j), \tag{A1}$$

where $\vec{e}_i$ and $\vec{e}_s$ are the polarization vectors of the incident and scattered x ray, $\hat{f}_j$ is the atomic scattering factor (ASF) tensor of the jth ion in the unit cell, $\vec{K} = \vec{k}_s - \vec{k}_i$, where $\vec{k}_i$ and $\vec{k}_s$ are the wave vectors of the incident and scattered x ray, and $\vec{d}_j$ is the position of the jth ion.[31,32] The intensity of RXS is proportional to $|S(k)|^2$.

In the present experiment, we detected the $(0k0)$ reflection (k is an odd number) of the x ray on the ac plane of $BaV_{10}O_{15}$. This $(0k0)$ reflection with odd k is forbidden in the normal Thomson scattering because of the existence of the b glide (along the bc plane) in the low-T phase (space group $Pbca$). Namely, the existence of ions at $\vec{d}_j$ and $\vec{d}_j + \vec{b}/2$, where $\vec{b}$ is the primitive vector along the b axis, contributes to the structure factor by the same magnitude but opposite signs for the $(0k0)$ reflection with odd k. However, in the RXS, some components of the ASF tensor $\hat{f}_j$ change their signs with the b glide operation, i.e., the mirror reflection in the bc plane, and the ions at $\vec{d}_j$ and $\vec{d}_j + \vec{b}/2$ can contribute to the structure factor with the same sign for the $(0k0)$ reflection (odd k) with an appropriate choice of $\vec{e}_i$ and $\vec{e}_s$ in Eq. (A1).

With the mirror reflection in the bc plane, i.e., with the transformation $a \to -a$, the tensor is transformed as

$$\begin{pmatrix} f_{aa} & f_{ab} & f_{ac} \\ f_{ba} & f_{bb} & f_{bc} \\ f_{ca} & f_{cb} & f_{cc} \end{pmatrix} \to \begin{pmatrix} f_{aa} & -f_{ab} & -f_{ac} \\ -f_{ba} & f_{bb} & f_{bc} \\ -f_{ca} & f_{cb} & f_{cc} \end{pmatrix}. \tag{A2}$$

Thus, if $\vec{e}_i$ and $\vec{e}_s$ are along the a and b axis, or along the a and c axis, we can "pick up" f_{ab} and f_{ac}, and two ions related by the b glide operation contributes to the structure factor by the same sign.

In the present experiment, when the azimuthal angle Ψ is 0°, $\vec{e}_i$ is along the a axis and $\vec{e}_s$ is approximately along the ab plane. Therefore, in this configuration, we can observe the $(0k0)$ reflection with odd k, whose intensity is dominated by f_{ab}. Equation (1) in the main text can be obtained from Eq. (A1) by assuming $\vec{e}_i \parallel a$, $\vec{e}_s \parallel b$, and $\vec{K} = (0k0)$.

2. Structure factor of $BaV_{10}O_{15}$

In the low-T phase of $BaV_{10}O_{15}$, a trimer is composed of three inequivalent V ions (V3B, V3, and V2B), and there are eight trimers in one unit cell. These eight trimers are related to each other by the a glide (with the $c \to -c$ mirror reflection), b glide (with the $a \to -a$ mirror reflection), c glide (with the $b \to -b$ mirror reflection) operation, or the combination of them.

In Fig. 5, we draw the V ions and trimers in a unit cell. The symmetric operations between eight V trimers are as follows:

(i) From $j = 1$ to 5: by the c glide (with $b \to -b$)

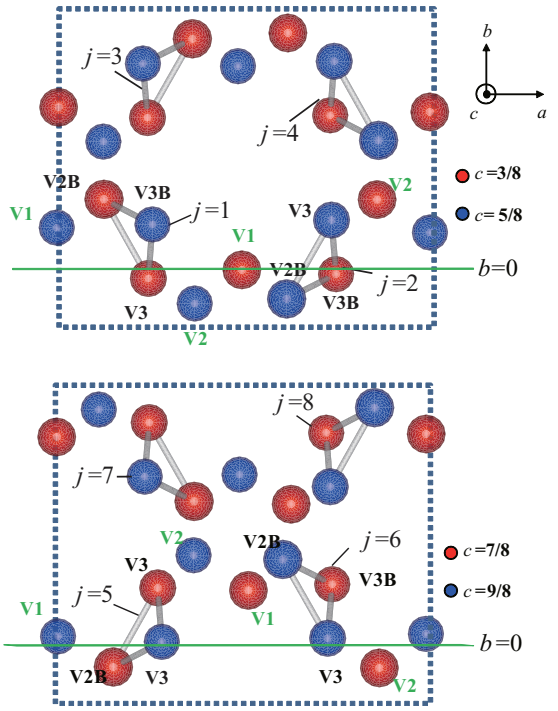

FIG. 5. (Color online) V ions of the low-T phase for $BaV_{10}O_{15}$. The bars connecting the spheres (V ions) represent the V-V bonds in trimers. The unit cell is indicated by dashed lines.

(ii) From $j = 1$ to 6: by the a glide (with $c \to -c$)

(iii) From $j = 5$ to 2: by the a glide (with $c \to -c$)

(iv) From $j = 1$ to 3, from $j = 2$ to 4, from $j = 5$ to 7, and from $j = 6$ to 8: by the b glide (with $a \to -a$).

The f_{ab} component, which we studied in the present experiment, changes its sign with $b \to -b$ or with $a \to -a$ but does not with $c \to -c$. Table II shows the list of the b position in the crystal and parity σ, which is the sign of f_{ab} arising from the glide operations for each V ion. Based on this, the structure factor for $(0k0)$ given in Eq. (1) can be written as

$$\begin{aligned} S(k) = {} & [-2 + 2\exp(i\pi k) + 2\exp(i\pi k/3) \\ & - 2\exp(-2i\pi k/3)] f_{ab}^{\mathrm{V3B}} \\ & + [2 - 2\exp(i\pi k) - 2\exp(i\pi k/3) \\ & + 2\exp(-2i\pi k/3)] f_{ab}^{\mathrm{V3}} \\ & + [2\exp(i\pi k/2) - 2\exp(-i\pi k/2) \\ & - 2\exp(-i\pi k/6) + 2\exp(5i\pi k/6)] f_{ab}^{\mathrm{V2B}}. \end{aligned} \tag{A3}$$

Here, f_{ab}^{V3B}, f_{ab}^{V3}, f_{ab}^{V2B} are the ASF tensors of the V trimer sites, V3B, V3, and V2B, respectively. The explicit forms of $S(k)$ for (010), (030), (050) are

$$\begin{aligned} S_{010} &= (-2 + 2\sqrt{3}i) f_{ab}^{\mathrm{V3B}} + (2 - 2\sqrt{3}i) f_{ab}^{\mathrm{V3}} \\ &\quad + (-2\sqrt{3} + 6i) f_{ab}^{\mathrm{V2B}}, \\ S_{030} &= -8 f_{ab}^{\mathrm{V3B}} + 8 f_{ab}^{\mathrm{V3}}, \\ S_{050} &= (-2 - 2\sqrt{3}i) f_{ab}^{\mathrm{V3B}} + (2 + 2\sqrt{3}i) f_{ab}^{\mathrm{V3}} \\ &\quad + (2\sqrt{3} + 6i) f_{ab}^{\mathrm{V2B}}. \end{aligned} \tag{A4}$$

TABLE II. b positions and the parity of the jth trimers in the unit cell.

α	j	b	σ	α	j	b	σ	α	j	b	σ
V3B	No. 1	2/12	+	V3	No. 1	0	+	V2B	No. 1	3/12	+
	No. 2	0	−		No. 2	2/12	−		No. 2	−1/12	−
	No. 3	8/12	−		No. 3	6/12	−		No. 3	9/12	−
	No. 4	6/12	+		No. 4	8/12	+		No. 4	5/12	+
	No. 5	0	−		No. 5	2/12	−		No. 5	− 1/12	−
	No. 6	2/12	+		No. 6	0	+		No. 6	3/12	+
	No. 7	6/12	+		No. 7	8/12	+		No. 7	5/12	+
	No. 8	8/12	−		No. 8	6/12	−		No. 8	9/12	−

APPENDIX B: CALCULATION DETAILS OF THE ASF TENSORS

1. Transformation matrix between the local and global coordinates

In this Appendix, we discuss how to calculate the ASF tensor of each V ion for each peak (pre-edge A, structure B, and main-edge C). In such a calculation, one often needs to transform vectors or tensors from the local $\vec{x}$, $\vec{y}$, $\vec{z}$ coordinates (each of which is along a V ion and a neighboring O ion) to the global $\vec{a}$, $\vec{b}$, $\vec{c}$ coordinates (which are along the crystal axes). Let us first discuss the transformation matrix between these two coordinates.

The left panel of Fig. 6 shows the V trimers composed of V3B, V3, and V2B in the crystal (in the global $\vec{a}$, $\vec{b}$, $\vec{c}$ coordinates), and the right panel shows the same trimer in the local $\vec{x}$, $\vec{y}$, $\vec{z}$ coordinates. For example, the displacement vector from V3 to V3B corresponds to an edge of the tetrahedron, and thus is given by $(0, \sqrt{3}/3, \sqrt{6}/3)$ in the global $\vec{a}$, $\vec{b}$, $\vec{c}$ coordinates. On the other hand, it is given by $(-\sqrt{2}/2, 0, \sqrt{2}/2)$ in the local $\vec{x}$, $\vec{y}$, $\vec{z}$ coordinates.

Based on such an argument, we can obtained the transformation matrix U, by which a vector is transformed from (a, b, c) to (x, y, z), where a vector $\vec{r}$ is given by $\vec{r} = a\vec{a} + b\vec{b} + c\vec{c} = x\vec{x} + y\vec{y} + z\vec{z}$:

$$U = \begin{pmatrix} -\frac{\sqrt{2}}{2} & \frac{\sqrt{6}}{6} & \frac{\sqrt{3}}{3} \\ 0 & -\frac{\sqrt{6}}{3} & \frac{\sqrt{3}}{3} \\ -\frac{\sqrt{2}}{2} & -\frac{\sqrt{6}}{6} & -\frac{\sqrt{3}}{3} \end{pmatrix} \tag{B1}$$

$$\sum_j U_{ij} a_j = x_i, \tag{B2}$$

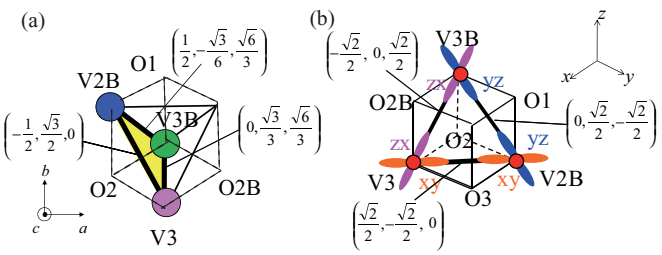

FIG. 6. (Color online) Displacement vectors between the trimer sites of V3B, V3, and V2B in the (a) global ($\vec{a}$, $\vec{b}$, $\vec{c}$) and (b) local ($\vec{x}$, $\vec{y}$, $\vec{z}$) coordinates.

where, $(a_1, a_2, a_3) = (a, b, c)$ and $(x_1, x_2, x_3) = (x, y, z)$. By this U, a tensor $\hat{A}$ in the global $\vec{a}$, $\vec{b}$, $\vec{c}$ coordinates is transformed to a tensor $\hat{X}$ in the local $\vec{x}$, $\vec{y}$, $\vec{z}$ coordinates as follows:

$$X_{kl} = \sum_{ij} U_{ki} U_{lj} A_{ij} = \sum_{ij} U_{ki} A_{ij} U^{\dagger}_{lj}, \tag{B3}$$

and thus,

$$A_{ij} = \sum_{kl} U^{\dagger}_{ik} X_{kl} U_{lj}. \tag{B4}$$

2. Calculation of the ASF tensors for main-edge C

In this section, the calculation of f^{α}_{ab} in the V ion for the main-edge C is discussed, which is similar to the method used in the study of $R\mathrm{TiO}_3$ by Nakao *et al.*[15] The ASF tensor for the main-edge peak C is related to the energy splitting of the $4p$ states of the transition-metal ions, which is dominated by the orbital states in the transition-metal sites.[14,15,26–28]

The ASF tensor has a form of a symmetric matrix,[31,32] and thus, with an appropriate choice of a Cartesian coordinate system, the tensor can be diagonalized as

$$\begin{pmatrix} f_1 & 0 & 0 \\ 0 & f_2 & 0 \\ 0 & 0 & f_3 \end{pmatrix}. \tag{B5}$$

When we calculate the structure factor by Eq. (1), this tensor should be transformed to the global $\vec{a}$, $\vec{b}$, $\vec{c}$ coordinate system.

Here, we made two assumptions. (1) $f_1 = f_2$ for all V3B, V3, and V2B, and (2) $f_3 - f_1$ is the same for all three V ions. These two assumptions can be justified as follows: Let us consider the case when the ASF tensor around the $1s$ to $4p$ transition is dominated by the $3d$ t_{2g} orbital ordering based on the model proposed by Ishihara *et al.*, where the Coulomb interaction between $4p$ and $3d$ is taken account of.[27] When there are two electrons in the t_{2g} state, as is the case in the present compound, if the two orbitals that are occupied by electrons are orthogonal to each other, the tensor can be diagonalized as Eq. (B5) with $f_1 = f_2$, by taking the intersection of the two planes for the two planer t_{2g} orbitals as the $\vec{z}'$ axis (principal axis). For example if one electron occupies the d_{xy} state and the other occupies the d_{yz} state, then the tensor can be diagonalized in the local $\vec{x}$, $\vec{y}$, $\vec{z}$ coordinates by taking the y direction as the principal axis of the tensor (for f_3) and z and y as the other two axes (for $f_1 = f_2$). Furthermore,

the Coulomb repulsion energy between the $4p$ and $3d$ orbital is the same as long as the relative angle between the two is the same. This justifies the assumption (2).

With the assumptions, the tensor of each V site can be diagonalized as

$$\begin{pmatrix} f & 0 & 0 \\ 0 & f & 0 \\ 0 & 0 & f+\Delta f \end{pmatrix} = fI + \Delta f \begin{pmatrix} 0 & 0 & 0 \\ 0 & 0 & 0 \\ 0 & 0 & 1 \end{pmatrix}, \quad \text{(B6)}$$

where I is the unit matrix, with a Cartesian coordinate system $\vec{x}'$, $\vec{y}'$, $\vec{z}'$. Since the first term remains the unit matrix with any transformation of the Cartesian coordinate, it does not contribute to the RXS intensity, and only the second term should be considered. If the $\vec{z}'$ axis (the principal axis) of the tensor in the Cartesian coordinates is given by (p, q, r) $(\sqrt{p^2+q^2+r^2}=1)$, the tensor in the second term of Eq. (B6) is transformed to

$$\Delta f \begin{pmatrix} 0 & 0 & 0 \\ 0 & 0 & 0 \\ 0 & 0 & 1 \end{pmatrix} \rightarrow \Delta f \begin{pmatrix} p^2 & pq & pr \\ pq & q^2 & qr \\ pr & qr & r^2 \end{pmatrix}. \quad \text{(B7)}$$

Thus, if $\Delta f = f_3 - f_1$ is the same for all the V ions, it becomes a constant factor of f^{α}_{ab} for any α, and $S(k)$ in Eq. (1) is dominated only by the value of pq for each V ion. In other words, only if we know the principal axis of the tensor for each V ion, we can calculate the intensity ratio of the (010), (030), and (050) for the main-edge C.

In the model of the orbital ordering by Pen *et al.*, d_{zx}, d_{yz} are occupied in V3B, d_{zx}, d_{xy} are occupied in V3, and d_{yz}, d_{xy} are occupied in V2B. Therefore, the directions of the principal axes for the ASF tensors of V3B, V3, and V2B are (0,0,1), (1,0,0), and (0,1,0) in the local coordinates, respectively. The ASF tensor of each V ion can be obtained by (B7) after transforming these principal axes to those in the global coordinates using (B1) and (B2), or equivalently, by using (B7) first with (p, q, r) in the local coordinates and then by transforming the tensor to that in the global coordinates using (B1) and (B4). The Q dependence of the relative intensity for the main-edge peak can be calculated by (A4) with f^{α}_{ab} (α = V3B, V3, and V2B) thus obtained.

3. Calculation of the ASF tensors for the pre-edge A and structure B

In this section, the calculation of f^{α}_{ab} in the V ion for the pre-edge A and structure B is discussed. If there is a complete centrosymmetry around the transition metal in the O_6 octahedra, the $1s$ to $3d$ (or $4s$) transition by a dipole transition is prohibited, and a quadrupole transition has to be taken into account. The RXS intensity arising from such a quadrupole transition will be much smaller than that arising from a dipole transition, and thus, the intensity of the pre-edge A will be much smaller than that of the main-edge C in such a case. This is inconsistent with the present experimental result. However, since the position of the V ion is off center in a O_6 octrahedron because of the V trimerization in the low-T phase of $BaV_{10}O_{15}$, there appears the electric dipole around the V ion. The appearance of the electric dipole is caused by the hybridization of a p state and the d (or s) state, and thus, the dipole transition becomes allowed between the $1s$ and $3d$ (or $4s$) state that is hybridized with the $4p$ state in the low-T phase of $BaV_{10}O_{15}$.

Here, we assume that the direction of the electric dipole is parallel to the displacement of the V ion from the center of the O_6 octahedron, and its size is proportional to the absolute value of the displacement. Experimentally, the displacement of the V ion [(p, q, r) in the global coordinates] can be obtained from the diffraction data.[7] This assumption means that the p state that is hybridized with the d (s) state is parallel in space to the direction of the displacement of the V ion, and the amount of the hybridization is proportional to the absolute value of the displacement.

The anisotropic ASF tensor f_{ab} at each site is given by

$$f_{ab} = -\frac{m}{e^2} \sum_l \frac{\langle f|\mathbf{O}^*_b|l\rangle\langle l|\mathbf{O}_a|0\rangle}{\varepsilon_0 - \varepsilon_l + E - i\Gamma}, \quad \text{(B8)}$$

where $|0\rangle$, $|f\rangle$ describes the initial and final states with the energy ε_0 and ε_f, $|l\rangle$ is the intermediate state with the energy ε_l, E is the energy of the x ray, and the vectors $\mathbf{O}_a$ and $\mathbf{O}^*_b$ describe the electric current operators of the dipole absorption,[27,31,32] which are parallel to the polarization of the incident and scattered x ray, respectively. Since in the present case, $|l\rangle$ corresponds to the p state parallel to the displacement of the V ion [(p, q, r) in the global coordinates], f_{ab} is proportional to the projections of the displacement of the V ion to the a axis (polarization of the incident x ray) multiplied by that to the b axis (polarization of the scattered x ray), i.e., pq. This is schematically illustrated in Fig. 7. Namely, only the value of pq for each V ion is relevant to the Q dependence of the pre-edge A or structure B.

This is equivalent to say that the ASF tensor for the dipole transition is diagonalized as

$$\begin{pmatrix} f_\perp & 0 & 0 \\ 0 & f_\perp & 0 \\ 0 & 0 & f_\parallel \end{pmatrix} = f_\perp I + (f_\parallel - f_\perp) \begin{pmatrix} 0 & 0 & 0 \\ 0 & 0 & 0 \\ 0 & 0 & 1 \end{pmatrix}, \quad \text{(B9)}$$

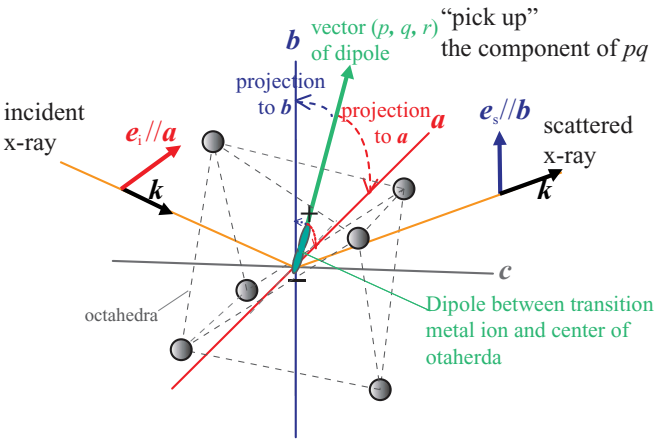

FIG. 7. (Color online) RXS arises from the electric dipole originating from the centrosymmetry breaking in the octahedra.

in the Cartesian coordinates in which the principal axis (for $f_{\parallel}$) is along the electric dipole and the other two axes (for $f_{\perp}$) are perpendicular to it. The second term in Eq. (B9) is transformed to the global coordinates similarly to Eq. (B7). Here, if the size of the displacement is the same for all three V ions, $f_{\parallel} - f_{\perp}$ is the same and only the direction of the electric dipole for each V ion is relevant to the Q dependence.

[1] M. Hase, I. Terasaki, and K. Uchinokura, Phys. Rev. Lett. **70**, 3651 (1993).

[2] P. G. Radaelli, New J. Phys. **7**, 53 (2005), and references therein.

[3] H. F. Pen, L. H. Tjeng, E. Pellegrin, F. M. F. de Groot, G. A. Sawatzky, M. A. van Veenendaal, and C. T. Chen, Phys. Rev. B **55**, 15500 (1997).

[4] N. Katayama, M. Uchida, D. Hashizume, S. Niitaka, J. Matsuno, D. Matsumura, Y. Nishihata, J. Mizuki, N. Takeshita, A. Gauzzi, M. Nohara, and H. Takagi, Phys. Rev. Lett. **103**, 146405 (2009).

[5] H. Kato, M. Kato, K. Yoshimura, and K. Kosuge, J. Phys. Soc. Jpn. **70**, 1404 (2001).

[6] G. Liu and J. E. Greedan, J. Solid State Chem. **122**, 416 (1996).

[7] C. A. Bridges, J. E. Greedan, and H. Kleinke, J. Solid State Chem. **177**, 4516 (2004).

[8] A. Bridges and J. E. Greedan, J. Solid State Chem. **177**, 1098 (2004).

[9] T. Kajita, T. Kanzaki, T. Suzuki, J. E. Kim, K. Kato, M. Takata, and T. Katsufuji, Phys. Rev. B **81**, 060405(R) (2010).

[10] J. Miyazaki, T. Sonehara, D. Akahoshi, H. Kuwahara, J. E. Kim, K. Kato, M. Takata, and T. Katsufuji, Phys. Rev. B **79**, 180410(R) (2009).

[11] M. Ikeda, T. Okuda, K. Kato, M. Takata, and T. Katsufuji, Phys. Rev. B **83**, 134417 (2011).

[12] J. Miyazaki, K. Matsudaira, Y. Shimizu, M. Itoh, Y. Nagamine, S. Mori, J. E. Kim, K. Kato, M. Takata, and T. Katsufuji, Phys. Rev. Lett. **104**, 207201 (2010).

[13] H. F. Pen, J. van den Brink, D. I. Khomskii, and G. A. Sawatzky, Phys. Rev. Lett. **78**, 1323 (1997).

[14] Y. Murakami, H. Kawada, H. Kawata, M. Tanaka, T. Arima, Y. Moritomo, and Y. Tokura, Phys. Rev. Lett. **80**, 1932 (1998).

[15] H. Nakao, Y. Wakabayashi, T. Kiyama, Y. Murakami, M. v. Zimmermann, J. P. Hill, D. Gibbs, S. Ishihara, Y. Taguchi, and Y. Tokura, Phys. Rev. B **66**, 184419 (2002).

[16] M. Noguchi, A. Nakazawa, S. Oka, T. Arima, Y. Wakabayashi, H. Nakao, and Y. Murakami, Phys. Rev. B **62**, R9271 (2000).

[17] L. Paolasini, C. Vettier, F. de Bergevin, F. Yakhou, D. Mannix, A. Stunault, W. Neubeck, M. Altarelli, M. Fabrizio, P. A. Metcalf, and J. M. Honig, Phys. Rev. Lett. **82**, 4719 (1999).

[18] T. Oguchi, Phys. Rev. B **51**, 1385 (1995).

[19] T. Oguchi, Phys. Rev. B **72**, 245105 (2005).

[20] T. Oguchi, J. Phys. Soc. Jpn. **78**, 044702 (2009).

[21] M. Fabrizio, M. Altarelli, and M. Benfatto, Phys. Rev. Lett. **80**, 3400 (1998).

[22] F. M. F. de Groot, Chem. Rev. **101**, 1779 (2001).

[23] J. Wong, F. W. Lytle, R. P. Messmer, and D. H. Maylotte, Phys. Rev. B **30**, 5596 (1984).

[24] O. Šipr, A. Šimůnek, S. Bocharov, T. Kirchner, and G. Dräger, Phys. Rev. B **60**, 14115 (1999).

[25] B. Poumellec, J. F. Marucco, and B. Touzelin, Phys. Rev. B **35**, 2284 (1987).

[26] M. Benfatto, Y. Joly, and C. R. Natoli, Phys. Rev. Lett. **83**, 636 (1999).

[27] S. Ishihara and S. Maekawa, Phys. Rev. Lett. **80**, 3799 (1998).

[28] I. S. Elfimov, V. I. Anisimov, and G. A. Sawatzky, Phys. Rev. Lett. **82**, 4264 (1999).

[29] The scattering angle is small and the effect of the surface roughness cannot be excluded in the present experiment.

[30] Y. Shimizu, K. Matsudaira, M. Itoh, T. Kajita, and T. Katsufuji, Phys. Rev. B **84**, 064421 (2011).

[31] D. H. Templeton and L. K. Templeton, Acta Cryst. A **36**, 237 (1980).

[32] V. E. Dmitrienko, Acta Cryst. A **39**, 29 (1983).